 CMES, vol.99, no.3, pp.233-253, 2014

Long-term Analyses of Concrete-Filled Steel Tubular Arches Accounting for Interval Uncertainty

Yong-Lin Pi[1] **and Mark Andrew Bradford**[1]

Abstract: Creep and shrinkage of the concrete core of a concrete-filled steel tubular (CFST) arch under sustained loading are inevitable, and cause a long-term change of the equilibrium configuration of the CFST arch. As the equilibrium configuration changes continuously, the long-term radial and axial displacements of the CFST arch, stress distributions as well as the internal forces in the steel tube and the concrete core change substantially with time. Creep and shrinkage of the concrete core are related to a number of its material parameters such as its creep coefficient, aging coefficient, and shrinkage strain. The values of these parameters differ significantly from one experiment to another, highlighting that these parameters experience certain amounts of uncertainty, which needs to be considered in the long-term analysis of a CFST arch. Although stochastic methods can be used to account for such uncertainties, their statistical variations are presumed being known, which have to be inferred from laboratory tests. However, the available data from creep and shrinkage tests of the concrete core of CFST members are quite limited and scattered, and so the stochastic method is of little use. This paper presents a long-term analysis of CFST circular arches by accounting for interval uncertainties in these parameters by interval modelling, and derives the upper and lower bounds for the long-term structural responses. It is shown that the uncertainties of creep and shrinkage of the concrete core have significant long-term effects on the structural behaviour of CFST arches.

Keywords: analysis, arches, concrete core, creep, interval, long-term, shrinkage, time-dependent, uncertainty

1 Introduction

Engineering applications of concrete-filled steel tubular arches are increasing rapidly, for example, more than 400 concrete-filled steel tubular (CFST) arch bridges

[1] The University of New South Wales, UNSW Sydney, NSW, Australia.

(Fig. 1) have been constructed worldwide hitherto [Pi, Liu, Bradford, and Zhang (2012)].

Figure 1: Concrete-filled steel tubular arch.

The cross-section of a CSFT arch (Fig. 2) consists of well bonded steel tube and concrete core and so the inevitable visco-elastic effects of creep and shrinkage of the concrete core may influence the structural behaviour of the CFST arch under a sustained load in the long-term [Bradford, Pi, and Qu (2011); Pi, Bradford, and Qu (2011)].

It is known that the final shrinkage strain and final creep coefficient of the concrete core play important roles in the long-term analyses of CFST arches [Bradford, Pi, and Qu (2011); Pi, Bradford, and Qu (2011)] when the age adjusted modulus method is used [ACI Committee 209 (1982); AS3600 (2003)]. Hence, it is essential to use the correct final shrinkage strain and final creep coefficient of the concrete core in the long-term analysis. Investigations of the creep and shrinkage parameters of the concrete core of straight CFST members [Terrey, Bradford, and Gilbert (1994); Uy (2001); L. H. Ichinose and E. Watanabe and H. Nakai (2001); Han, Tao, and Liu (2004)] have shown that because the egress of moisture of the concrete core is prevented by the steel tube, the final shrinkage strain and final creep coefficient are smaller than those of plain concrete, and that the value of the final shrinkage strain and final creep coefficient obtained from experiments reported by different researchers varies scatteringly over a quite large range as shown in Table 1. Hence, it is questionable to treat these parameters as being deterministic. To account for the large variations of the final shrinkage strain and final creep coefficient, they should be treated as uncertain parameters.

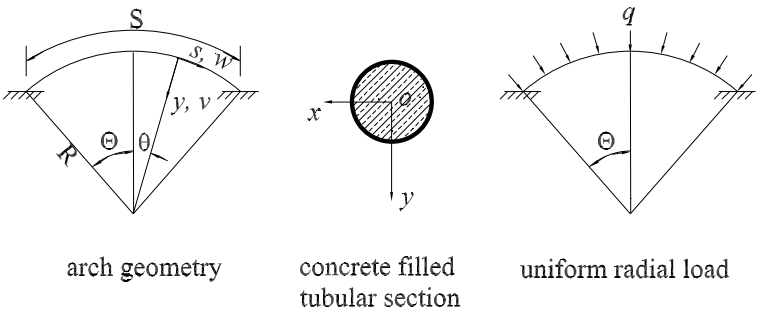

Figure 2: Geometry and loading for concrete-filled steel tubular arch.

Table 1 Final shrinkage strain and final creep coefficient

	final shrinkage strain (10^{-6})	final creep coefficient
Terrey et al.	50	1.0
Uy	340	2.0
Ichinose et al.	63	1.16-1.26
Han et al.	45.3	0.836

The routine stochastic method is usually used to account for such uncertainties, which requires the statistical parameters of the uncertain final shrinkage strain and final creep coefficient to be derived from experiments. Currently available data from such experiments, however, are quite limited and scattered as shown in Table 1. Therefore, it is difficult to derive their probabilistic distributions, probability density functions, and/or spectral density from the limited and scattered data and so the stochastic method is difficult to be used to consider uncertainties of the final shrinkage strain and final creep coefficient. The experimental results [Terrey, Bradford, and Gilbert (1994); Uy (2001); L. H. Ichinose and E. Watanabe and H. Nakai (2001); Han, Tao, and Liu (2004)] show that the uncertain final shrinkage strain and final creep coefficient vary within bounded intervals. In this case, a mathematical discipline, viz. interval analysis [Moore, Kearfott, and Cloud (2009)], can be used to account for bounded uncertainties of the final shrinkage strain and final creep coefficient and to perform the interval uncertainty analysis for the long-term behaviour of CFST arches under a sustained load. The interval analysis has been used by a number of researchers to account for uncertainties and it has been shown

that the interval analysis is useful for structural uncertain analyses [Moore, Kearfott, and Cloud (2009); Gao (2007)].

This paper, therefore, presents an in-plane long-term structural analysis of CFST circular arches due to creep and shrinkage of the concrete core with interval uncertain final creep coefficient and final shrinkage strain under a sustained uniform radial load (Fig. 2), which represents a new technique for modelling uncertainties in the long-term analysis of CFST arches and provides a sound understanding of the effect of uncertain creep and shrinkage of the concrete core on the long-term behaviour of CFST arches.

2 Creep and Shrinkage of Concrete Core

One of the difficulties in studying the long-term structural behaviour of CFST arches is that there is no definitive exact model available for concrete shrinkage and creep, although the visco-elastic effects of concrete shrinkage and creep on concrete structures have been studied widely [Gilbert and Ranzi (2011)]. A number of methods for the shrinkage and creep of concrete have been developed and proposed [Bažant and Cedolin (2003); Abdulrazeg, Noorzaei, Khanehzaei, Jaafar, and Mohammed (2010); Ishizawa and Iura (2006); Ferretti and Di Leo (2008); Luo, Pi, Gao, and Bradford (2013); Jang, Son, and Kwon (2013)]. Although each method has its own merits, it has been shown that the age-adjusted effective modulus method is efficient, can provide quite accurate predictions for the creep of concrete, and can be easily incorporated into structural analyse. This method uses algebraic formulas to model the creep and shrinkage of concrete and is recommended by ACI Committee 209 (1982) and the Australian Design Standard for Concrete Structures AS3600 (2003). Hence, the age-adjusted effective modulus method is used for the shrinkage and creep of the concrete core in this investigation. With this method, the total strain $\varepsilon(t,t_0)$ of the instantaneous and creep strains, and the strain increment produced by restrained creep can be expressed as

$$\varepsilon(t,t_0) = \frac{\sigma_0}{\bar{E}_{ec}(t,t_0)} + \frac{\Delta\sigma(t,t_0)}{E_{ec}(t,t_0)}, \tag{1}$$

in which the time t is in days, σ_0 is the stress at time $t = t_0$ corresponding to the instantaneous strain, $\Delta\sigma(t,t_0)$ is the gradual change of stress after time $t = t_0$, $E_{ec}(t,t_0)$ and $\bar{E}_{ec}(t,t_0)$ are the effective modulus of concrete including creep effects and the age-adjusted effective modulus of concrete respectively and they are given by ACI Committee 209 (1982), AS3600 (2003), Gilbert and Ranzi (2011), and Bažant and Cedolin (2003)

$$\bar{E}_{ec}(t,t_0) = \frac{E_c}{1+\phi(t,t_0)} \quad \text{and} \quad E_{ec}(t,t_0) = \frac{E_c}{1+\chi(t,t_0)\phi(t,t_0)} \tag{2}$$

with E_c being Young's modulus of concrete.

In these equations, $\phi(t,t_0)$ is the creep coefficient and $\chi(t,t_0)$ is the aging coefficient and they are given by

$$\phi(t,t_0) = \left[\frac{(t-t_0)^{0.6}}{10+(t-t_0)^{0.6}}\right]\phi_u \text{ and } \chi(t,t_0) = 1 - \frac{(1-\chi^*)(t-t_0)}{20+(t-t_0)} \tag{3}$$

respectively, in which ϕ_u is the final creep coefficient and $\phi_u = 1.25t_0^{-0.118}\phi_{\infty,7}$ with $\phi_{\infty,7}$ being the creep coefficient at time infinity when the first loading time is $t = 7$ days after the concrete casting, and

$$\chi^* = \frac{k_1 t_0}{k_2 + t_0} \text{ with } k_1 = 0.78 + 0.4e^{-1.33\phi_{\infty,7}} \text{ and } k_2 = 0.16 + 0.8e^{-1.33\phi_{\infty,7}}. \tag{4}$$

It is noted that when $t = t_0$, $\chi(t_0,t_0) = 1$ and so $\bar{E}_{ec}(t_0,t_0) = E_{ec}(t_0,t_0)$

Because egress of moisture of the concrete core is prevented by the steel tube, the value of the creep coefficient of ϕ_u or $\phi_{\infty,7}$ should be taken for the moist curing condition of the concrete, or it can be obtained from shrinkage and creep tests of CFST members.

3 Determination of Bounds for Interval Shrinkage and Creep

To determine the final shrinkage strain and the final creep coefficient of the concrete core, several researchers [Terrey, Bradford, and Gilbert (1994); Uy (2001); L. H. Ichinose and E. Watanabe and H. Nakai (2001); Han, Tao, and Liu (2004)] have performed experiments on shrinkage and creep of CFST members. It has been found that because the egress of the moisture of the concrete core is prevented by the steel tube, the final shrinkage strain ε_{sh}^* and the final creep coefficient ϕ_u are smaller than those of plain concrete. However, the value of the final shrinkage strain ε_{sh}^* and the final creep coefficient ϕ_u obtained by different tests varies significantly because the factors that influence the shrinkage and creep of the concrete core are complicated. This indicates that it is difficult to choose proper deterministic values of the final shrinkage strain ε_{sh}^* and the final creep coefficient ϕ_u. Hence, to predict the effects of creep and shrinkage of the concrete core properly, the uncertainties of the values of the final shrinkage strain ε_{sh}^* and the final creep coefficient ϕ_u have to be considered in the analysis. The uncertainties of these properties can be treated by using stochastic analyses of structures. However, because the test results for the final shrinkage strain ε_{sh}^* and the final creep coefficient ϕ_u of the concrete cores of CFST members are quite limited and scattered, it is rather difficult to estimate experimentally their probabilistic distribution, probability density function, or the spectral density function of the stochastic variations of the creep and shrinkage

properties. The test results reported by several researchers (Table 1) [Terrey, Bradford, and Gilbert (1994); Uy (2001); L. H. Ichinose and E. Watanabe and H. Nakai (2001); Han, Tao, and Liu (2004)] show that the values of the final creep coefficient ϕ_u and the final shrinkage strain ε^*_{sh} of the concretes core of CFST members are bounded. Hence, the intervals [Moore, Kearfott, and Cloud (2009)] of the final shrinkage strain and the final creep coefficient are herein used to account for their uncertainties. In this study, the value of the final creep coefficient ϕ_u is assumed to vary in the interval from 1.0 to 2.0, while the value of the final shrinkage strain ε^*_{sh} is assumed to vary from 150×10^{-6} to 340×10^{-6}, which are used for the interval uncertain long-term analysis for CFST arches in this paper and can be expressed by intervals as $\phi^I_u=[1.0,2.0]$ and $\varepsilon^{*\,I}_{sh}=[150\times10^{-6},340\times10^{-6}]$ (see Appendix A.1).

Based on the interval final creep coefficient ϕ^I_u, the interval creep coefficient $\phi(t,t_0)^I$ can be obtained by extending the creep coefficient function $\phi(t,t_0)$ given by Eq. (3) into an interval function (Appendix A.2) as

$$\phi(t,t_0)^I=[\phi_1(t,t_0),\phi_2(t,t_0)] \tag{5}$$

with

$$\phi_1(t,t_0)=\frac{(t-t_0)^{0.6}\phi_{u1}}{10+(t-t_0)^{0.6}}\ \text{ and }\ \phi_2(t,t_0)=\frac{(t-t_0)^{0.6}\phi_{u2}}{10+(t-t_0)^{0.6}}. \tag{6}$$

The interval aging coefficient $\chi(t,t_0)^I$ can be obtained by extending the aging coefficient function $\chi(t,t_0)$ given by Eq. (3) into an interval function as

$$\chi(t,t_0)^I=[\chi_1(t,t_0),\chi_2(t,t_0)] \tag{7}$$

where

$$\chi_1(t,t_0)=1-\frac{[1-\chi^*_1](t-t_0)}{20+(t-t_0)}\ \text{ and }\ \chi_2(t,t_0)=1-\frac{[1-\chi^*_2](t-t_0)}{20+(t-t_0)} \tag{8}$$

with χ^*_1 and χ^*_2 being the lower and upper bounds of the interval parameter $(\chi^*)^I$ and given by

$$\chi^*_1=\frac{k_{11}t_0}{k_{22}+t_0}\ \text{ and }\ \chi^*_2=\frac{k_{12}t_0}{k_{21}+t_0}, \tag{9}$$

in which k_{11} and k_{12} are the lower and upper bounds of the interval parameter k^I_1, while k_{21} and k_{22} are the lower and upper bounds of the interval parameter k^I_1.

The interval parameters k^I_1 and k^I_2 are defined by

$$k^I_1=[k_{11},k_{12}]=0.78+0.4e^{-1.33\phi^I_{\infty,7}},\ \ k^I_2=[k_{21},k_{22}]=0.16+0.8e^{-1.33\phi^I_{\infty,7}}. \tag{10}$$

respectively, in which the interval variable $\phi^I_{\infty,7}$ is given by $\phi^I_{\infty,7} = t_0^{0.118}\phi^I_u/1.25 = t_0^{0.118}[0.8, 1.6]$.

The time dependent modulus of the concrete core given by Eq. (2) can be extended to the interval long-term modulus as

$$E^I_{ec}(t,t_0) = \left[\frac{E_c}{1+\chi_2(t,t_0)\phi_2(t,t_0)}, \frac{E_c}{1+\chi_1(t,t_0)\phi_1(t,t_0)}\right] \tag{11}$$

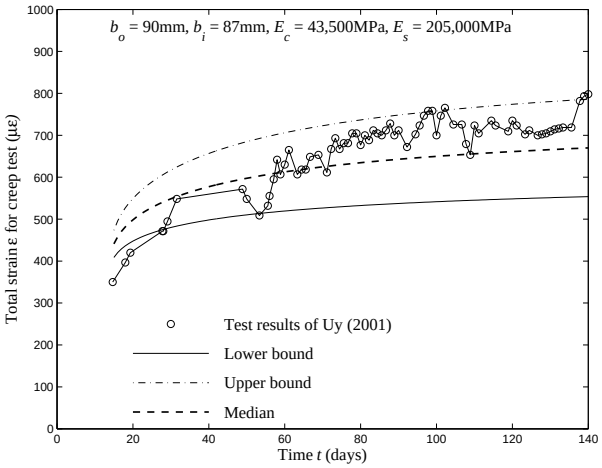

Figure 3: Comparison with long-term test results of Uy (2001).

Because there are no tests on the creep and shrinkage behaviour of CFST arches reported in the open literature, to verify the proposed interval model for the final creep coefficient and the final shrinkage strain of the concrete core, the predictions for the long-term behaviour of CFST columns under sustained axial compression are compared with test results of Uy (2001) and Han, Tao, and Liu (2004) for CFST columns in Figs. 3 and 4 respectively. Uy (2001) performed long-term tests of short CFST box columns under sustained axial compression. A $b_o = 90$ mm square steel tube with a wall-thickness of $t = 3$ mm was used. The first loading time was 14 days after concrete core casting. The sustained load of 15 MPa was applied over the surface area of the CFST column and produced a strain of 350 $\mu\varepsilon$. The test time was 140 days. The elastic modulus of the concrete core and steel tube are $E_c = 43,500$ MPa and $E_s = 205,000$ MPa. Han, Tao, and Liu (2004) also carried out long-term tests of four CFST box columns under sustained axial compression. A $b_o = 100$ mm square steel tube with a wall-thickness of $t = 2.3$ mm was used.

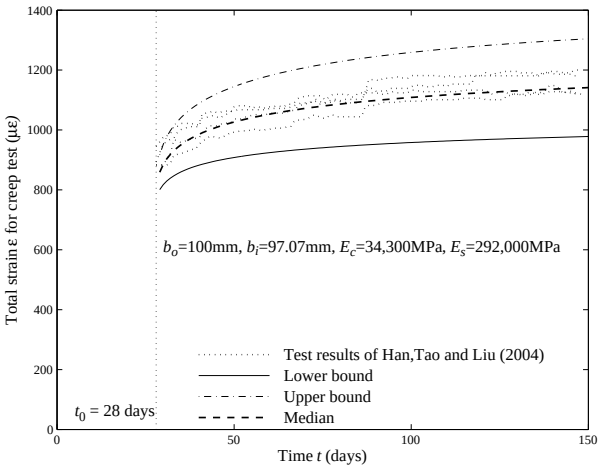

Figure 4: Comparison with long-term test results of Han, Tao, and Liu (2004).

The first loading time was 28 days after concrete core casting. The sustained axial load of $Q = 360$ kN was applied. The elastic modulus of the concrete core and steel tube are $E_c = 34,300$ MPa and $E_s = 292,000$ MPa. It can be seen from Fig. 3 and 4 that the test results of the strain of the CFST column have some uncertainty and vary in an interval and that the uncertain long-term strain responses predicted by the interval uncertain analysis can closely define the lower and upper bounds of the test results. The median obtained by the interval analysis can also be used to predict the long-term strains of CSFT columns.

4 Long-Term Analysis Accouting for Interval Uncertaity

4.1 Long-Term Differential Equation of Equilibrium

The basic assumptions adopted in the present investigation are: (1) Deformations of the CFST arch are elastic and satisfy the Euler-Bernoulli hypothesis, i.e. the cross-section remains plane and perpendicular to the arch axis during deformation. (2) The arches are assumed to be slender, i.e. the dimensions of the cross-section are much smaller than the length and radius of the arch. (3) The steel tube is bonded fully with the concrete core.

The differential equations of equilibrium for the in-plane long-term behaviour analysis of a CFST arch can be derived as [Bradford, Pi, and Qu (2011)]

$$r_e^2(\tilde{v}^{iv} + \tilde{w}''') - R^2\left[\tilde{w}' - \tilde{v} + \frac{A_c E_{ec}\varepsilon_{sh}}{A_s E_s + A_c E_{ec}}\right] - \frac{qR^3}{A_s E_s + A_c E_{ec}} = 0 \tag{12}$$

in the radial direction, and

$$r_e^2(\tilde{v}''' + \tilde{w}'') + R^2(\tilde{w}'' - \tilde{v}') = 0 \tag{13}$$

in the axial direction, and the static boundary condition for pin-ended arches can also be derived as [Bradford, Pi, and Qu (2011)]

$$\tilde{v}'' + \tilde{w}' = 0 \quad \text{at} \quad \theta = \pm\Theta \tag{14}$$

where the time t and initial time t_0 are dropped for simplification (i.e. $E_{ec} = E_{ec}(t,t_0)$ et al.), dimensionless long-term displacements $\tilde{v}$ and $\tilde{w}$ are defined by $\tilde{v} = v/R$ and $\tilde{w} = w/R$, v and w are the long-term radial and axial displacements in the directions of axes oy and os respectively (Fig. 2), R is the radius of initial curvature of the arch, $(\,)' \equiv \mathrm{d}(\,)/\mathrm{d}\theta$, $(\,)'' \equiv \mathrm{d}^2(\,)/\mathrm{d}\theta^2$, θ is the angular coordinate, and A_c and A_s, and I_c and I_s, are the area and second moment of area of the concrete core and steel tube respectively, the long-term radius of gyration of the effective cross-section r_e about its major principal axis is defined by $r_e = \sqrt{(E_sI_s + E_{ec}I_c)/(A_sE_s + A_cE_{ec}}$, and ε_{sh} is the shrinkage strain of the concrete core and can be expressed as

$$\varepsilon_{sh} = \left(\frac{t}{t+d}\right)\varepsilon_{sh}^*. \tag{15}$$

The essential kinematic boundary conditions are

$$\tilde{v} = 0, \;\; \tilde{w} = 0 \;\; \text{and} \;\; \tilde{v} = 0, \;\; \tilde{v}' = 0, \;\; \tilde{w} = 0 \;\; \text{at} \;\; \theta = \pm\Theta \tag{16}$$

for pin-ended and fixed arches, respectively.

4.2 Long-term Displacements with Interval Uncertainty

The long-term radial and axial displacements $\tilde{v}$ and $\tilde{w}$ can be obtained by solving Eqs. (12) and (13) simultaneously and using the boundary conditions given by Eqs. (14) and (16) as

$$\tilde{v} = \frac{A_cE_{ec}\varepsilon_{sh} + qR}{(A_sE_s + A_cE_{ec})\Phi_P}\{(R^2 + r_e^2)(\Theta K_1 - \theta\sin\theta\sin\Theta)$$

$$+ [(R^2 - r_e^2)\sin\Theta - 2R^2\Theta\cos\Theta]K_2\}, \tag{17}$$

and

$$\tilde{w} = \frac{A_cE_{ec}\varepsilon_{sh} + qR}{(A_sE_s + A_cE_{ec})\Phi_P}[(R^2 + r_e^2)K_3 + 2R^2\cos\Theta K_4] \tag{18}$$

with $K_1 = (1-\cos\theta\cos\Theta)$, $K_2 = \cos\theta - \cos\Theta$, $K_3 = \theta\sin\Theta\cos\theta - \Theta\sin\theta\cos\Theta$ and $K_4 = \theta\sin\Theta - \Theta\sin\theta$ for pin-ended arches, with the long-term parameter Φ_P being given by

$$\Phi_P = (\cos\Theta\sin\Theta + \Theta)r_e^2 + (\Theta + 2\Theta\cos^2\Theta - 3\cos\Theta\sin\Theta)R^2; \tag{19}$$

and

$$\tilde{v} = \frac{A_c E_{ec}\varepsilon_{sh} + qR}{(A_s E_s + A_c E_{ec})\Phi_F}\Theta(R^2 + r_e^2)[\Theta K_1 + \sin\Theta(\cos\Theta - \cos\theta - \theta\sin\theta)], \tag{20}$$

$$\tilde{w} = \frac{A_c E_{ec}\varepsilon_{sh} + qR}{(A_s E_s + A_c E_{ec})\Phi_F}[(R^2 + r_e^2)\Theta K_3 + 2R^2\sin\Theta K_4] \tag{21}$$

for fixed arches, with the long-term parameter Φ_F being given by

$$\Phi_F = (R^2 + r_e^2)\Theta(\Theta + \cos\Theta\sin\Theta) - 2R^2\sin^2\Theta. \tag{22}$$

Because the displacements given by Eqs. (17), (18), (20), and (21) are real functions of the effective modulus E_{ec}, shrinkage strain ε_{sh} of the concrete core, and the long-term parameters r_e, Φ_P, and Φ_F, based on the theorem about the extension of real functions to interval functions (Appendix A.2) [Moore, Kearfott, and Cloud (2009)], they can be extended to interval functions of the long-term displacements and so the interval long-term radial and axial displacements $\tilde{v}^I$ and $\tilde{w}^I$ can be obtained using the interval operations (Appendix A.1) as

$$\tilde{v}^I = [\tilde{v}_1,\ \tilde{v}_2] \quad \text{and} \quad \tilde{w}^I = [\tilde{w}_1,\ \tilde{w}_2]. \tag{23}$$

For pin-ended arches, the upper and lower bounds of the interval long-term radial and axial displacements $\tilde{v}^I$ and $\tilde{w}^I$ can be obtained by extending the deterministic solutions (17) and (18) as

$$\begin{aligned}
\tilde{v}_1 &= \tfrac{A_c E_{ec1}\varepsilon_{sh1} + qR}{(A_s E_s + A_c E_{ec2})\Phi_{P2}}\{[R^2 + r_{e1}^2][\Theta(1-\cos\theta\cos\Theta) - \theta\sin\theta\sin\Theta] \\
&\quad + [(R^2 - r_{e2}^2)\sin\Theta - 2R^2\Theta\cos\Theta](\cos\theta - \cos\Theta)\} \\
\tilde{v}_2 &= \tfrac{A_c E_{ec2}\varepsilon_{sh2} + qR}{(A_s E_s + A_c E_{ec1})\Phi_{P1}}\{[R^2 + r_{e2}^2][\Theta(1-\cos\theta\cos\Theta) - \theta\sin\theta\sin\Theta] \\
&\quad + [(R^2 - r_{e1}^2)\sin\Theta - 2R^2\Theta\cos\Theta](\cos\theta - \cos\Theta)\}
\end{aligned} \tag{24}$$

and

$$\begin{aligned}
\tilde{w}_1 &= \tfrac{A_c E_{ec1}\varepsilon_{sh1} + qR}{(A_s E_s + A_c E_{ec2})\Phi_{P2}}[(R^2 + r_{e1}^2)K_3 + 2R^2\cos\Theta K_4] \\
\tilde{w}_2 &= \tfrac{A_c E_{ec2}\varepsilon_{sh2} + qR}{(A_s E_s + A_c E_{ec1})\Phi_{P1}}[(R^2 + r_{e2}^2)K_3 + 2R^2\cos\Theta K_4]
\end{aligned} \tag{25}$$

with the long-term interval parameter Φ_P^I being given by

$$\Phi_P^I = [\Phi_{P1}, \Phi_{P2}] = (\cos\Theta\sin\Theta + \Theta)[r_{e1}^2, r_{e2}^2] + (\Theta + 2\Theta\cos^2\Theta - 3\cos\Theta\sin\Theta)R^2.$$

(26)

For fixed arches, the upper and lower bounds of the long-term radial and axial displacements $\tilde{v}^I$ and $\tilde{w}^I$ can be obtained by extending the deterministic solutions (20) and (21) as

$$\begin{array}{l} \tilde{v}_1 = \frac{A_c E_{ec1} \varepsilon_{sh1} + qR}{(A_s E_s + A_c E_{ec2})\Phi_{F2}} \Theta(R^2 + r_{e1}^2)[\Theta K_1 + \sin\Theta(\cos\Theta - \cos\theta - \theta\sin\theta)] \\ \tilde{v}_2 = \frac{A_c E_{ec2} \varepsilon_{sh2} + qR}{(A_s E_s + A_c E_{ec1})\Phi_{F1}} \Theta(R^2 + r_{e2}^2)[\Theta K_1 + \sin\Theta(\cos\Theta - \cos\theta - \theta\sin\theta)] \end{array}, \tag{27}$$

and

$$\begin{array}{l} \tilde{w}_1 = \frac{A_c E_{ec1} \varepsilon_{sh1} + qR}{(A_s E_s + A_c E_{ec2})\Phi_{F2}} [(R^2 + r_{e1}^2)\Theta K_3 + 2R^2 \sin\Theta K_4] \\ \tilde{w}_2 = \frac{A_c E_{ec2} \varepsilon_{sh2} + qR}{(A_s E_s + A_c E_{ec1})\Phi_{F1}} [(R^2 + r_{e2}^2)\Theta K_3 + 2R^2 \sin\Theta K_4] \end{array} \tag{28}$$

with the interval long-term parameter Φ_F^I being given by

$$\Phi_F^I = [\Phi_{F1}, \Phi_{F2}] = \left\{R^2 + [r_{e1}^2, r_{e2}^2]\right\} \Theta(\Theta + \cos\Theta\sin\Theta) - 2R^2 \sin^2\Theta. \tag{29}$$

Typical lower and upper bounds and median of the dimensionless long-term central radial displacement under a sustained uniform radial load given by Eq. (23) are shown as variations of the dimensionless central creep radial displacements $v_{c,t}/v_{c,15}$ with time t in Figs. 5a and 5b for pin-ended and fixed arches respectively, where a sustained uniform load $q = 100$ kN/m is applied at time $t_0 = 15$ days after concrete casting, and $v_{c,t}$ and $v_{c,15}$ are the central radial displacements at time t and t_0, respectively. The material properties were assumed as: the elastic moduli of the steel and concrete $E_s = 200,000$ MPa and $E_c = 30,000$ MPa and the geometries of the arches were assumed as: the arch span $L = 15$m, and the included angle of the arch $2\Theta = 120^\circ$. The cross-section of the steel tube is assumed to be circular with the outer radius $r_o = 250$ mm and the inner radius $r_i = 240$ mm. For comparison, the results of the deterministic analysis given by Eqs. (17) and (20) using the lower and upper bound values of the final shrinkage strain and final creep coefficient are also shown in Figs. 5a and 5b. In the interval analysis, the interval numbers for the final creep coefficient and the final shrinkage strain $\phi^I = [1.0, 2.0]$ and $\varepsilon_{sh}^I = [150 \times 10^{-6}, 340 \times 10^{-6}]$ are used, while the upper bounds $\phi = 2.0$ and 340×10^{-6} and the lower bound $\phi = 1.0$ and $\varepsilon_{sh} = 150 \times 10^{-6}$ are used for the deterministic analysis to obtain the upper and lower bound results. It can be seen from Figs. 5a and 5b that the upper bound and even the median of dimensionless long-term displacements obtained by the interval uncertainty analysis is higher than the upper bound obtained by the deterministic analysis. Hence, the deterministic analysis may lead to underestimated and unsafe predictions for the long-term radial displacements even when the upper bound values of the final shrinkage strain

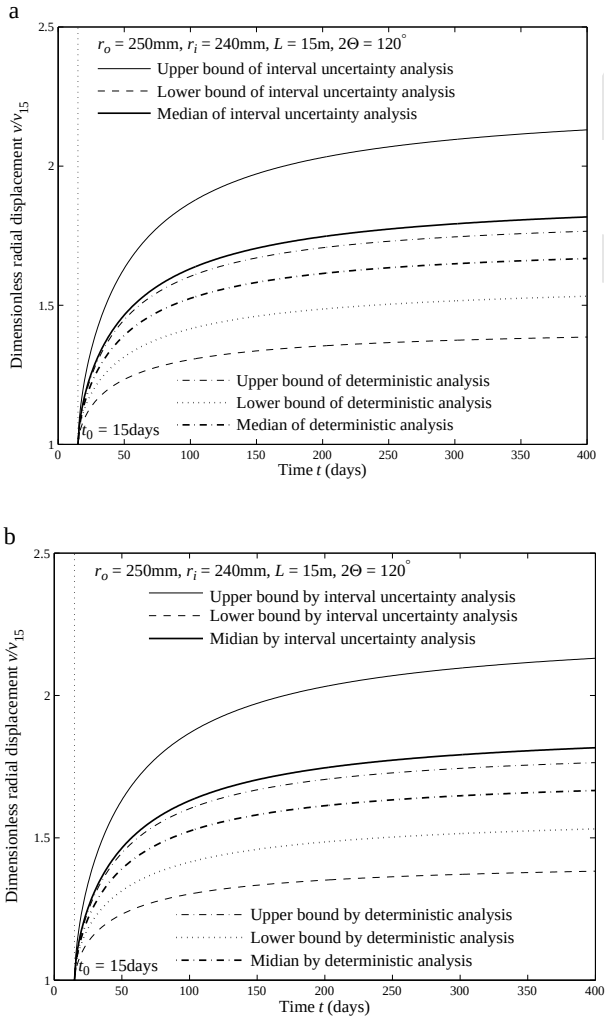

Figure 5: long-term central radial displacement.

and final coefficient are used. The upper bounds of the interval analysis predict the worst case of the long-term radial displacements, which at the time $t = 400$ days is about 2.2 times of that at the time $t_0 = 15$ days and this may violate serviceability of CFST arches in the long-term. Because of this, in the service limit state design, sufficient reserve for the radial displacement should be provided.

4.3 Long-Term Stresses in Steel Tube and Concrete Core with Interval Uncertainty

The long-term stresses σ_s in the steel tube and σ_c in the concrete core can be expressed as [Bradford, Pi, and Qu (2011)]

$$\sigma_s = E_s\varepsilon = E_s\left[\tilde{w}' - \tilde{v} - \frac{y(\tilde{v}''+\tilde{w}')}{R}\right] \tag{30}$$

and

$$\sigma_c = E_{ec}(\varepsilon+\varepsilon_{sh}) = E_{ec}\left[\tilde{w}' - \tilde{v} - \frac{y(\tilde{v}''+\tilde{w}')}{R} + \varepsilon_{sh}\right]. \tag{31}$$

Substituting the solutions of the long-term displacements $\tilde{v}$ and $\tilde{w}$ given by Eqs. (17) and (18) into the stress expressions given by Eqs. (30) and (31) leads to

$$\sigma_s = -\frac{E_s(A_cE_{ec}\varepsilon_{sh}+qR)}{A_cE_{ec}+A_sE_s} + \frac{2E_s(qR+A_cE_{ec}\varepsilon_{sh})\sin\Theta[r_e^2\cos\theta+yRK_2]}{(A_sE_s+A_cE_{ec})\Phi_P} \tag{32}$$

and

$$\sigma_c = -\frac{E_{ec}(qR-A_sE_s\varepsilon_{sh})}{A_cE_{ec}+A_sE_s} + \frac{2E_c(qR+A_cE_{ec}\varepsilon_{sh})\sin\Theta[r_e^2\cos\theta+yRK_2]}{(A_sE_s+A_cE_{ec})\Phi_P} \tag{33}$$

for pin-ended CFST arches; and

$$\sigma_s = -\frac{E_s(A_cE_{ec}\varepsilon_{sh}+qR)}{A_cE_{ec}+A_sE_s} + \frac{2E_s(qR+A_cE_{ec}\varepsilon_{sh})\sin\Theta[r_e^2\Theta\cos\theta-yRK_5]}{(A_sE_s+A_cE_{ec})\Phi_F} \tag{34}$$

and

$$\sigma_c = -\frac{E_{ec}(qR-A_sE_s\varepsilon_{sh})}{A_cE_{ec}+A_sE_s} + \frac{2E_{ec}(qR+A_cE_{ec}\varepsilon_{sh})\sin\Theta[r_e^2\Theta\cos\theta-yRK_5]}{(A_sE_s+A_cE_{ec})\Phi_F} \tag{35}$$

for fixed CFST arches, where $K_5 = \Theta\cos\theta - \sin\Theta$.

Because the stresses given by Eqs. (32)-(35) are real functions of the final shrinkage strain and final creep coefficient of the concrete core, the interval long-term stresses σ_s^I in the steel tube and σ_c^I in the concrete core can be obtained by using the interval operations (Appendix A.1) to extend the deterministic solutions for stresses as

$$\sigma_s^I = [\sigma_{s1}, \sigma_{s2}] \quad \text{and} \quad \sigma_c^I = [\sigma_{c1}, \sigma_{c2}]. \tag{36}$$

For pin-ended arches, the lower and upper bounds of σ_s^I in the steel tube are given by

$$\begin{aligned}
\sigma_{s1} &= \frac{2E_s(qR+A_cE_{ec1}\varepsilon_{sh1})\sin\Theta(r_{e1}^2\cos\theta+yRK_2)}{(A_sE_s+A_cE_{ec2})\Phi_{P2}} - \frac{E_s(A_cE_{ec2}\varepsilon_{sh2}+qR)}{A_cE_{ec1}+A_sE_s} \\
\sigma_{s2} &= \frac{2E_s(qR+A_cE_{ec2}\varepsilon_{sh2})\sin\Theta(r_{e2}^2\cos\theta+yRK_2)}{(A_sE_s+A_cE_{ec1})\Phi_{P1}} - \frac{E_s(A_cE_{ec1}\varepsilon_{sh1}+qR)}{A_cE_{ec2}+A_sE_s}
\end{aligned} \tag{37}$$

and the lower and upper bounds of σ_c^I in the concrete core are given by

$$\begin{aligned}\sigma_{c1} &= \frac{2E_{ec1}(qR+A_cE_{ec1}\varepsilon_{sh1})\sin\Theta[r_{e1}^2\cos\theta+yRK_2)]}{(A_sE_s+A_cE_{ec2})\Phi_{P2}} - \frac{E_{ec2}(qR-A_sE_s\varepsilon_{sh1})}{A_cE_{ec1}+A_sE_s}\\ \sigma_{c2} &= \frac{2E_{ec2}(qR+A_cE_{ec2}\varepsilon_{sh2})\sin\Theta[r_{e2}^2\cos\theta+yRK_2]}{(A_sE_s+A_cE_{ec1})\Phi_{P1}} - \frac{E_{ec1}(qR-A_sE_s\varepsilon_{sh2})}{A_cE_{ec2}+A_sE_s}\end{aligned} \quad . \tag{38}$$

For fixed arches, the upper and lower bounds of interval long-term stresses σ_s^I and σ_c^I in the steel tube and concrete core can be obtained by extending the deterministic solutions (34) and (35) as

$$\begin{aligned}\sigma_{s1} &= \frac{2E_s(qR+A_cE_{ec1}\varepsilon_{sh1})\sin\Theta[r_{e1}^2\Theta\cos\theta-yRK_5]}{(A_sE_s+A_cE_{ec2})\Phi_{F2}} - \frac{E_s(A_cE_{ec2}\varepsilon_{sh2}+qR)}{A_cE_{ec1}+A_sE_s}\\ \sigma_{s2} &= \frac{2E_s(qR+A_cE_{ec2}\varepsilon_{sh2})\sin\Theta[r_{e2}^2\Theta\cos\theta-yRK_5)]}{(A_sE_s+A_cE_{ec1})\Phi_{F1}} - \frac{E_s(A_cE_{ec1}\varepsilon_{sh1}+qR)}{A_cE_{ec2}+A_sE_s}\end{aligned} \tag{39}$$

and

$$\begin{aligned}\sigma_{c1} &= \frac{2E_{ec1}(qR+A_cE_{ec1}\varepsilon_{sh1})\sin\Theta[r_{e1}^2\Theta\cos\theta-yRK_5]}{(A_sE_s+A_cE_{ec2})\Phi_{F2}} - \frac{E_{ec2}(qR-A_sE_s\varepsilon_{sh1})}{A_cE_{ec1}+A_sE_s}\\ \sigma_{c2} &= \frac{2E_{ec2}(qR+A_cE_{ec2}\varepsilon_{sh2})\sin\Theta[r_{e2}^2\Theta\cos\theta-yRK_5]}{(A_sE_s+A_cE_{ec1})\Phi_{F1}} - \frac{E_{ec1}(qR-A_sE_s\varepsilon_{sh2})}{A_cE_{ec2}+A_sE_s}\end{aligned} \quad . \tag{40}$$

Typical upper and lower bounds and median of interval long-term stresses in the steel tube and concrete core are shown in Figs. 6a and 6b as variations of of stresses σ_s and σ_c with the time, where σ_s and σ_c are stresses at the top interface between the concrete core and steel tube at the arch crown. A sustained uniform radial load $q = 100$ kN/m was applied. The median of the stresses obtained from the deterministic analysis are also shown in Figs. 6a and 6b. It can be seen that the creep and shrinkage of the concrete core increase the stresses in the steel tube significantly. The absolute values of the median of stresses σ_s in the steel tube obtained by the interval uncertain analysis are higher than those obtained by the deterministic analysis. When the uncertainties of the final creep coefficient and final shrinkage strain are considered, the stress in the steel tube may increase by more than 2 times from the first loading day $t_0 = 15$ days to $t = 400$ days. Because of this, a CFST arch that does not experience local buckling of steel tube plate may have local buckling of steel plate in the long-term [Uy (1998)]. If the sustained load is high, the steel tube may even yield. To avoid local buckling and yielding of the steel tube in the long-term, the CFST arches should have sufficient strength reserve in the strength limit state design. Because the upper bound of long-term stresses in the steel tube is very high, local buckling of steel tube may occur in the long-term.

4.4 Axial Forces and Bending Moments with Interval Uncertainty

The long-term axial force N and bending moment M can be obtained by substituting the stresses given by Eqs. (32) and (33), and Eqs. (34) and (35) as

$$N = -\int_{A_s}\sigma_s dA - \int_{A_c}\sigma_c dA = qR - \frac{2(qR+A_cE_{ec}\varepsilon_{sh})r_e^2\sin\Theta\cos\theta}{\Phi_P} \tag{41}$$

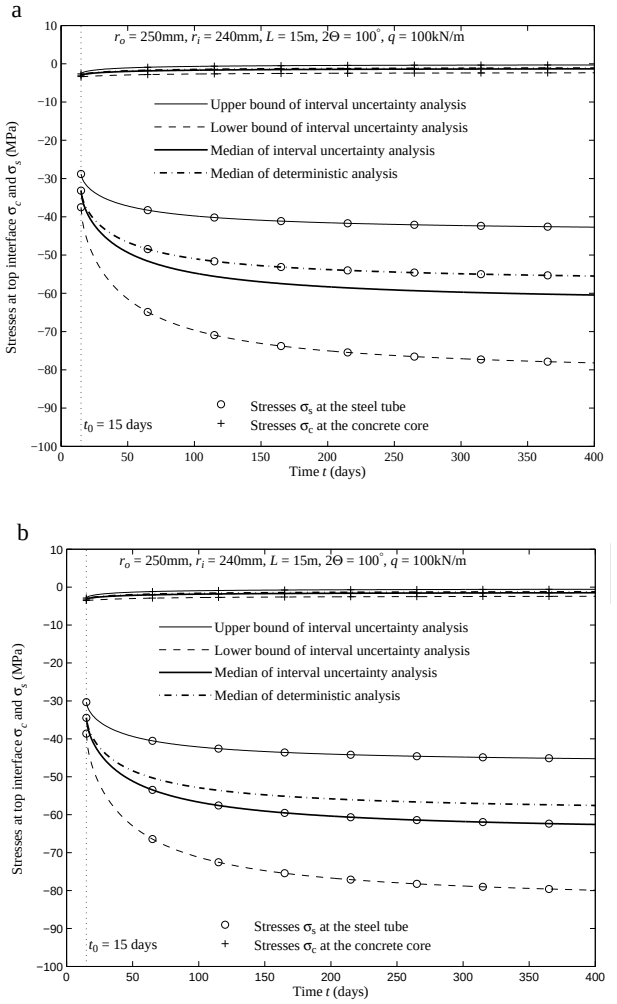

Figure 6: Interval long-term stresses at the arch crown.

and

$$M = \int_{A_s} \sigma_s y \mathrm{d}A + \int_{A_c} \sigma_c y \mathrm{d}A = \frac{2Rr_e^2 \sin\Theta(qR + A_c E_{ec} \varepsilon_{sh})(\cos\theta - \cos\Theta)}{\Phi_P} \tag{42}$$

for pin-ended arches, and

$$N = -\int_{A_s} \sigma_s \mathrm{d}A - \int_{A_c} \sigma_c \mathrm{d}A = qR - \frac{2(qR + A_c E_{ec} \varepsilon_{sh}) r_e^2 \Theta \sin\Theta \cos\theta}{\Phi_F} \tag{43}$$

and

$$M = \int_{A_s} \sigma_s y \mathrm{d}A + \int_{A_c} \sigma_c y \mathrm{d}A = \frac{2Rr_e^2 \sin\Theta(qR + A_c E_{ec}\varepsilon_{sh})(\Theta\cos\theta - \sin\Theta)}{\Phi_F} \tag{44}$$

for fixed arches.

Based on the deterministic solutions and the interval analysis theory [Moore, Kearfott, and Cloud (2009)], the interval long-term axial compressive force and bending moment can be expressed as

$$N^I = [N_1, N_2], \tag{45}$$

with

$$\begin{aligned} N_1 &= qR - \frac{2(qR + A_c E_{ec1}\varepsilon_{sh1}) r_{e1}^2 \sin\Theta\cos\theta}{\Phi_{P2}} \\ N_2 &= qR - \frac{2(qR + A_c E_{ec2}\varepsilon_{sh2}) r_{e2}^2 \sin\Theta\cos\theta}{\Phi_{P1}} \end{aligned} \tag{46}$$

and

$$M^I = [\frac{2R(qR + A_c E_{ec1}\varepsilon_{sh1}) r_{e1}^2 \sin\Theta K_2}{\Phi_{P2}}, \frac{2R(qR + A_c E_{ec2}\varepsilon_{sh2}) r_{e2}^2 \sin\Theta K_2}{\Phi_{P1}}] \tag{47}$$

for pin-ended arches; and

$$N^I = [N_1, N_2] \tag{48}$$

with

$$\begin{aligned} N_1 &= qR - \frac{2(qR + A_c E_{ec1}\varepsilon_{sh1}) r_{e1}^2 \Theta\sin\Theta\cos\theta}{\Phi_{F2}} \\ N_2 &= qR - \frac{2(qR + A_c E_{ec2}\varepsilon_{sh2}) r_{e2}^2 \Theta\sin\Theta\cos\theta}{\Phi_{F1}} \end{aligned} \tag{49}$$

and

$$M^I = [\frac{2R(qR + A_c E_{ec1}\varepsilon_{sh1}) r_{e1}^2 \sin\Theta K_5}{\Phi_{F2}}, \frac{2R(qR + A_c E_{ec2}\varepsilon_{sh2}) r_{e2}^2 \sin\Theta K_5}{\Phi_{F1}}] \tag{50}$$

for fixed arches.

The typical upper and lower bounds of the uncertain long-term central moment obtained from the interval uncertain analysis are shown in Figs. 7a and 7b, where the upper and lower bounds of the deterministic long-term central moment were obtained by considering the upper and lower bounds of the final shrinkage strain and final creep coefficient as deterministic parameters, respectively. It can be seen from Figs. 7a and 7b that the upper bound and median from the interval uncertainty analysis is higher than the upper bound from the deterministic analysis. Hence, the deterministic analysis may lead to underestimated results for the long-term bending moments even when the upper bound value of the final shrinkage strain and final creep coefficient is used.

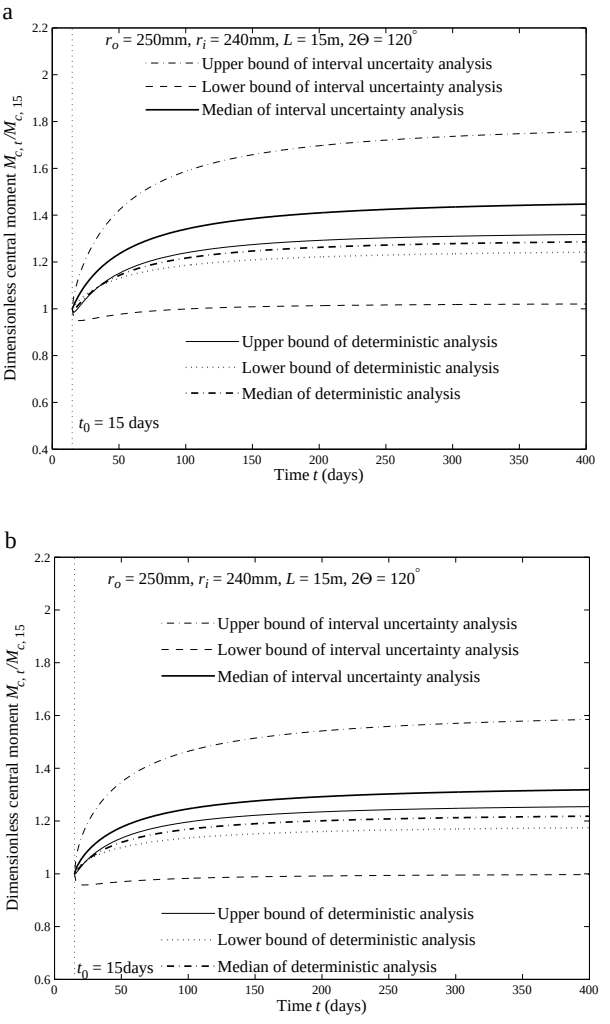

Figure 7: long-term central bending moment.

5 Conclusions

This paper presented the interval uncertain analysis of the long-term in-plane behaviour of CFST circular arches due to creep and shrinkage of the concrete core that are subjected to a sustained uniform radial load. It has been found that the interval analysis is useful and effective for accounting for the uncertainty of the final shrinkage strain and final creep coefficient of the concrete core in prediction of the long-term structural responses of CFST arches. The medians of structural

responses such as displacements, stresses, and bending moments from the internal uncertain analysis are higher than those from the deterministic analysis. In many cases, the median of structural responses predicted by the interval uncertain analysis are even higher than the upper bound of the deterministic results. This indicated that the deterministic analysis is not reliable even when the upper bound values of the final shrinkage strain and final creep coefficient of the concrete core are used.

The interval analysis has shown that the uncertainties of creep and shrinkage of the concrete core have significant effects on the long-term in-plane structural behaviour of CFST arches. The long-term displacements increase with time substantially. This increase, particularly the upper bound, is so large that it may affect the serviceability of the CFST arch. The long-term compressive stresses in the steel tube increase with time while the stresses in the concrete core decrease and even change from compressive to tensile as time increases. The upper bound of stresses are so higher that the local compressive strength reserve of the steel tube and the local tensile strength reserve of the concrete core may be affected.

Acknowledgement: This work has been supported by the Australian Research Council through Discovery Projects (DP120104554, DP130102934 and DP140101-887) awarded to both authors and an Australian Laureate Fellowship (FL100100063) awarded to the second author.

Appendix-A Mathematical background

Appendix-A.1 Interval Arithmetic Operations

An interval number means a closed bounded set of real numbers, defined by Moore, Kearfott, and Cloud (2009)

$$X^I = [x_1, x_2] = \{x : x_1 \leq x \leq x_2, x_1, x_2 \in \mathscr{R}\} \tag{51}$$

where $\mathscr{R}$ is a set of real number, X^I is a set of number and is called an interval, and x_1 and x_2 are the endpoints of the set (or of the interval). The interval has a dual nature of both the set and the number, representing a set of numbers by a new kind of number. For the convenience of operation, the median and the deviation (or radius) of an interval can be defined as

$$x^m = \frac{x_1 + x_2}{2} \quad \text{and} \quad \Delta x = \frac{x_2 - x_1}{2} \tag{52}$$

respectively. An interval X^I can then be expressed by

$$x^I = [x^m - \Delta x, x^m + \Delta x] = x^m + \Delta x e_{\Delta x} \quad \text{with} \quad e_{\Delta x} = [-1, 1] \tag{53}$$

where the interval $\Delta x e_{\Delta x}$ is the uncertainty interval of the interval X^I.
The arithmetic operations of two intervals X^I and Y^I can be defined as

$$X^I + Y^I = [x_1,\ x_2] + [y_1,\ y_2] = [x_1 + y_1,\ x_2 + y_2] \tag{54}$$

$$X^I - Y^I = [x_1,\ x_2] - [y_1,\ y_2] = [x_1 - y_2,\ x_2 - y_1] \tag{55}$$

$$\begin{aligned} X^I \times Y^I &= [x_1,\ x_2] \times [y_1,\ y_2] \\ &= [\min(x_1y_1, x_1y_2, x_2y_1, x_2y_2), \max(x_1y_1, x_1y_2, x_2y_1, x_2y_2)] \end{aligned} \tag{56}$$

$$\frac{X^I}{Y^I} = \frac{[x_1,\ x_2]}{[y_1,\ y_2]} = [x_1,\ x_2] \times [\frac{1}{y_2}, \frac{1}{y_1}]. \tag{57}$$

It is noted that

$$X^I - X^I = x^m[-1, 1] \tag{58}$$

from which, only when $x_1 = x_2$, i.e., the radius of the interval X^I vanishes as $X^I - X^I = [0, 0]$, and that

$$\frac{X^I}{X^I} = \begin{cases} \left[\frac{x_1}{x_2}, \frac{x_2}{x_1}\right] & \text{when} \quad x_1 \geq 0 \\ \left[\frac{x_2}{x_1}, \frac{x_1}{x_2}\right] & \text{when} \quad x_2 \leq 0 \end{cases} \tag{59}$$

from which, only when $x_1 = x_2$, $X^I / X^I = [1, 1]$.

Appendix-A.2 Interval Function

An interval function $F(X_1^I, X_2^I, ..., X_n^I)$ of n interval variables $X_1^I, X_2^I, ..., X_n^I$ is inclusion monotonic [Moore, Kearfott, and Cloud (2009)] if

$$Y_i^I \supseteq X_i^I \quad (i = 1, 2, ..., n) \tag{60}$$

implies that

$$F(Y_1^I, Y_2^I, ..., Y_n^I) \supseteq F(X_1^I, X_2^I, ..., X_n^I). \tag{61}$$

If an interval function is inclusion monotonic, the interval calculation of the function can be simplified. If $f(x_1, x_2, ..., x_n)$ is assumed to be a real function of n real variables $x_1, x_2, ..., x_n$, its interval extension is an interval valued function $F(X_1^I, X_2^I, ..., X_n^I)$ of n interval variables $X_1^I, X_2^I, ..., X_n^I$ with the property

$$F(x_1, x_2, ..., x_n) = f(x_1, x_2, ..., x_n) \quad \text{for all } x_1 \in X_1^I, x_2 \in X_2^I, ..., x_n \in X_n^I. \tag{62}$$

In other words, an interval extension of a real function is an interval valued function which has real value when the arguments are all real and coincides with the real function.

For a real rational function of real variables, the real variables can be replaced by the corresponding interval variables and the real arithmetic operations can be replaced by the corresponding interval arithmetic operations. As a result, the real rational function has been extended to a rational interval function, and then an interval value of F contains the range of values of the corresponding real function f when the real arguments of f are in the intervals of the interval variables of F.

References

Abdulrazeg, A. A.; Noorzaei, J.; Khanehzaei, P.; Jaafar, M. S.; Mohammed, T. A. (2010): Effect of Temperature and Creep on Roller Compacted Concrete Dam During the Construction Stages. *CMES: Computer Modeling in Engineering & Sciences*, vol. 68, no. 3, pp. 239–268.

ACI Committee 209 (1982): *Prediction of creep, shrinkage and temperature effects in concrete structures*. American Concrete Institute, Detroit.

AS3600 (2003): *Concrete structures*. Standards Australia, Sydney.

Bažant, Z. P.; Cedolin, L. (2003): *Stability of structures*. Dover Publications, Mineola, USA.

Bradford, M. A.; Pi, Y.-L.; Qu, W. L. (2011): Time-dependent in-plane behaviour and buckling of concrete-filled steel tubular. *Engineering Structures*, vol. 33, pp. 1781–1795.

Ferretti, E.; Di Leo, A. (2008): Cracking and Creep Role in Displacements at Constant Load: Concrete Solids in Compression. *CMES: Computer Modeling in Engineering & Sciences*, vol. 7, no. 2, pp. 59–80.

Gao, W. (2007): Finite element analysis of structures with interval parameters. *Journal of Mechanics*, vol. 23, no. 1, pp. 79–85.

Gilbert, R. I.; Ranzi, G. (2011): *Time-dependent behaviour of concrete structures*. Spon Press, London.

Han, L. H.; Tao, Z.; Liu, W. (2004): Effects of sustained load on concrete-filled hollow structural steel columnss. *Journal of Structural Engineering ASCE*, vol. 130, no. 9, pp. 1392–1404.

Ishizawa, T.; Iura, M. (2006): Analysis of Partially Concrete-Filled Steel Tubular Columns subjected to Cyclic Loadings. *CMES: Computer Modeling in Engineering & Sciences*, vol. 11, no. 3, pp. 121–130.

Jang, K. P.; Son, J. K.; Kwon, S. H. (2013): Prediction of Interfacial Cracking due to Differential Drying Shrinkage of Concrete in Precast Shell Pier Cap. *CMC: Computer, Materials & Continua*, vol. 38, no. 3, pp. 155–173.

L. H. Ichinose and E. Watanabe and H. Nakai (2001): An experimental study on creep of concrete filled steel pipes. *Journal of Constructional Steel Research*, vol. 57, pp. 453–466.

Luo, K.; Pi, Y.-L.; Gao, W.; Bradford, M. A. (2013): Creep of Concrete Core and Time-Dependent Non-Linear Behaviour and Buckling of Shallow Concrete-Filled Tubular Arches. *CMES: Computer Modeling in Engineering & Sciences*, vol. 95, no. 1, pp. 155–173.

Moore, R. E.; Kearfott, R. B.; Cloud, M. J. (2009): *Introduction to Interval Analysis*. Society for Industrial and Applied Mathematics, Philadelphia.

Pi, Y.-L.; Bradford, M. A.; Qu, W. L. (2011): Long-term non-linear behaviour and buckling of shallow concrete-filled steel tubular arches. *International Journal of Non-Linear Mechanics*, vol. 46, no. 1, pp. 1155–1166.

Pi, Y.-L.; Liu, C. Y.; Bradford, M. A.; Zhang, S. M. (2012): In-plane strength of concrete-filled steel tubular circular arches. *Journal of Constructional Steel Research*, vol. 69, no. 1, pp. 77–94.

Terrey, P. J.; Bradford, M. A.; Gilbert, R. I. (1994): Creep and shrinkage of concrete in concrete-filled circular steel tubes. In *Proceedings of 6th International Symposium on Tubular Structures*, pp. 293–296. Melbourne.

Uy, B. (1998): Local and post-local buckling of concrete filled steel welded box columns. *Journal of Constructional Steel Research*, vol. 47, no. 1, pp. 47–72.

Uy, B. (2001): Static long-term effects in short concrete-filled steel box columns under sustained loading. *ACI Structural Journal*, vol. 98, no. 1, pp. 96–104.